JGR Space Physics

RESEARCH ARTICLE
10.1029/2025JA033856

Control of Solar Wind on Magnetic Field Fluctuations in the Subsolar Magnetosheath

Ying Zou[1], Brian M. Walsh[2], Yuxi Chen[3], Hongyang Zhou[4], and Savvas Raptis[1]

[1]Johns Hopkins University Applied Physics Laboratory, Laurel, MD, USA, [2]Department of Mechanical Engineering, Center for Space Physics, Boston University, Boston, MA, USA, [3]Department of Climate and Space Sciences and Engineering, University of Michigan, Ann Arbor, MI, USA, [4]Department of Astronomy and Center for Space Physics, Boston University, Boston, MA, USA

Abstract The magnetosheath modifies the solar wind and IMF before they reach Earth's magnetosphere, and hence plays a crucial role in regulating the solar wind-magnetosphere interaction. Although the steady component of the magnetosheath magnetic field has been reasonably well reproduced, the fluctuating component has been less accounted for despite its significant amplitude. This paper empirically determines the mean characteristics of the ultra-low-frequency magnetic field fluctuations, and constructs a functional form using solar wind parameters. We use 15 years of THEMIS A data for the magnetosheath, and OMNI for the upstream solar wind conditions. Qualitatively, fluctuations are negatively correlated with the IMF cone angle, and positively with the solar wind speed and dynamic pressure. Some fluctuations are correlated with the IMF strength but not all. The level of fluctuations in the IMF is positively correlated with <0.01 Hz fluctuations in the magnetosheath. A higher Mach number is associated with a larger fraction of compressional versus transverse fluctuations in the magnetosheath. Quantitatively, the correlation between magnetosheath fluctuations and individual solar wind parameters is weak, correlation magnitude being <0.5. However, by performing a multiple linear regression fit of the solar wind parameters to magnetosheath fluctuations, a reasonably good prediction can be achieved with correlation magnitude in the range of 0.5–0.7, except for the parallel magnetosheath fluctuations of 0.01–0.1 Hz. Our results are overall consistent with earlier studies, but our quantitative approach further permits forecast of how much the IMF changes inside the magnetosheath which is beneficial for scientific understanding and space weather forecasts.

Key Points:

- The median characteristics of magnetosheath magnetic field fluctuations are determined and studied as a function of solar wind parameters
- Fluctuations are negatively (positively) correlated with the IMF cone angle (solar wind speed), with <0.5 correlation magnitude
- Improved prediction is achieved with a functional form combining solar wind parameters as constructed through multiple linear regression

Supporting Information:

Supporting Information may be found in the online version of this article.

Correspondence to:

Y. Zou,
ying.zou@jhuapl.edu

Citation:

Zou, Y., Walsh, B. M., Chen, Y., Zhou, H., & Raptis, S. (2025). Control of solar wind on magnetic field fluctuations in the subsolar magnetosheath. *Journal of Geophysical Research: Space Physics*, *130*, e2025JA033856. https://doi.org/10.1029/2025JA033856

Received 18 FEB 2025
Accepted 22 MAY 2025

1. Introduction

The magnetosheath is the interface between the flowing solar wind and the standing Earth's magnetosphere. It is bounded upstream by the bow shock and downstream by the magnetopause. The bow shock decelerates and compresses the solar wind, and the magnetopause diverts the flow, where the embedded magnetic field lines drape tangentially to the magnetopause. The magnetosheath, therefore, modifies the solar wind plasma and IMF variations before they reach the magnetosphere, playing a crucial role in regulating the solar wind-magnetosphere interaction. The plasma and magnetic field parameters inside the magnetosheath have been widely described by the gas dynamics or magnetohydrodynamic (MHD) models (e.g., Lyon, 1994; Spreiter et al., 1966; Siscoe et al., 2002; Wu, 1992), and statistical representation of in situ measurements (e.g., Dimmock & Nykyri, 2013; Paularena et al., 2001; Walsh et al., 2012; Zhang et al., 2019). However, these descriptions often deviate from the observed magnetosheath conditions (Pulinets et al., 2012; Rakhmanova et al., 2015, 2016; Šafránková et al., 2009; Walsh et al., 2019). For instance, Pulinets et al. (2012) compared the magnetic field in the subsolar magnetosheath and in the solar wind, and found that even under quasi-steady solar wind conditions, the sign of the B_z component differs in 30% of cases.

One important contributor to the discrepancies are fluctuations that populate the magnetosheath over a wide frequency range. The magnetosheath can be described as having a steady state and a fluctuating component. The steady state component is comparatively well correlated with the solar wind (Rakhmanova et al., 2015, 2016). The fluctuations, however, are less well-understood, despite their significant amplitude (reaching several tenths of the steady component). Magnetosheath fluctuations may influence magnetospheric phenomena by analogy with fluctuations in the solar wind, which enhance energy transfer across the magnetopause boundary (Ala-Lahti et al., 2024; Borovsky & Funsten, 2003; D'Amicis et al., 2007; Osmane et al., 2015). Possible sources of magnetosheath fluctuations include solar wind fluctuations, foreshock waves, and waves generated at the bow

shock or magnetopause, as well as instabilities inside the magnetosheath (Fairfield, 1976), many of which are missing in MHD models. Hybrid models (Karimabadi et al., 2014; Lu et al., 2020; Omidi et al., 2014; Palmroth et al., 2018) have successfully captured the fluctuating component of the magnetosheath, but the computational complexity limits the application of such models to only finite sets of upstream conditions. Hybrid models also only reproduce the fluctuations related to ion motion, waves, and instabilities. Empirical determination of the mean characteristics of magnetosheath fluctuations, and how the characteristics varies with the upstream conditions is therefore very helpful. Since the solar wind is the ultimate driver of the system and solar wind measurements are available nearly all the time, knowledge of the relation between the solar wind and magnetosheath fluctuations is in demand.

Fairfield and Ness (1970) observed that the magnetosheath exhibits highly variable magnetic fluctuations. The fluctuations change substantially from day to day, and those in the dawnside magnetosheath are overall larger than those in the duskside. Fairfield and Ness (1970) did not have the benefit of simultaneous solar wind measurement, and could not unambiguously determine what contributes to the large variations. Luhmann et al. (1986) considered the control of IMF, and found that the fluctuations are large on the dayside for small IMF cone angles, and large at dawn or dusk for large cone angles. Here the cone angle is defined as the angle between the IMF direction and the Sun-Earth line, and it is an important parameter because a large cone angle moves the quasi-parallel shock—and thus the disturbed magnetosheath behind it—away from the dayside to dawn/dusk. Luhmann's association between a quasi-parallel shock and magnetosheath fluctuations can be understood that shocks reflect a portion of the incoming ions back into the upstream plasma. In quasi-perpendicular shocks, the reflected ions are turned around by the magnetic field, whereas in quasi-parallel shocks, reflected ions move along the magnetic field lines traveling upstream, exciting waves and turbulence which are then blown by the solar wind into the magnetosheath. The Luhmann et al. (1986) result also explains, at least partly, the high fluctuations in the dawnside magnetosheath seen by Fairfield and Ness (1970) because the spiral oriented IMFs are frequently parallel to the dawnside shock normal. Following studies by Shevyrev et al. (2003, 2007) and Shevyrev and Zastenker (2005) confirmed the strong preference of magnetosheath fluctuations to downstream of quasi-parallel shocks.

Dimmock et al. (2014) suggested that magnetosheath fluctuations can be further enhanced during southward IMFs and during fast solar wind speeds. Under time periods of southward IMFs, subsolar reconnection produces flux transfer events (FTEs) (Russell & Elphic, 1979) that propagate tailward, and the magnetic field lines surrounding the FTEs would be perturbed manifesting as fluctuations. However, the north/south direction of the IMF seems to only affect the perpendicular component not the parallel component of the magnetic field. During high solar wind speeds, electromagnetic waves such as mirror mode, ion cyclotron, and whistler waves are enhanced downstream of collisionless shocks (Wilson et al., 2013), which possibly leads to an increased level of turbulence. Although the aforementioned studies mainly focused on the magnetic fluctuations, similar spatial and solar wind dependence has been reported for ion flux. For instance, Němeček et al. (2002) found that fluctuations of the magnetosheath ion flux show dawn-dusk asymmetry and preference to quasi-parallel shocks.

Fluctuations still occur behind quasi-perpendicular shocks, but these fluctuations are qualitatively different from those behind quasi-parallel shocks: the latter often correspond to developed turbulence with a power spectrum slope close to $-5/3$, whereas the former often correspond to locally generated waves with a much steeper spectrum slope (Shevyrev & Zastenker, 2005). Two common wave modes are the mirror mode waves and Alfvén-ion cyclotron (AIC) waves, also named electromagnetic ion cyclotron (EMIC) waves (Schwartz et al., 1996). The generation of these waves closely depends on local plasma conditions, particularly plasma beta and ion temperature anisotropy, which in turn depend on the driving solar wind conditions and the local properties of the shock. Soucek et al. (2015) showed that both waves tend to occur behind quasi-perpendicular shocks due to the high temperature anisotropy there. However, mirror waves are common during high (>7) Mach number conditions, and EMIC common during low (<7) Mach number conditions. Génot et al. (2009) suggested that the orientation of the IMF in the ecliptic plane also matters: mirror wave occurrence is higher when IMF is directed perpendicular to the average Parker spiral. Large-scale hybrid-Vlasov simulations show a consistent occurrence pattern (Hoilijoki et al., 2016).

Despite the efforts listed above, quantitative knowledge of how much the magnetosheath fluctuates under given solar wind conditions is still missing. The present paper quantifies the magnetic field fluctuations in the magnetosheath, mainly at ultra-low frequencies (ULF, ranging from 1 mHz to 1 Hz), by developing a functional form

using solar wind parameters. This information is essential for a quantitative prediction of how much the IMF changes inside magnetosheath before reaching the magnetosphere, and hence an assessment of the role of small-scale processes inside the magnetosheath in the solar wind-magnetosphere coupling. The information is also beneficial to space weather forecasts because small scale fluctuations can then be incorporated to MHD models which otherwise tend to only reproduce the steady state component of the magnetosheath. Hybrid models, although capable of capturing the fluctuating magnetosheath, have been challenging to validate because the stochastic nature of the fluctuations makes them highly irreproducible for distinct cases. Knowledge of the mean characteristics of the fluctuations, and how they vary with various background conditions, will help to evaluate the output of hybrid models. With solar wind parameters consistently available, a functional relationship to magnetosheath fluctuations can be established over a wide range of driving conditions.

Note that the aforementioned studies covered magnetic fluctuations of various ULF ranges. For instance, the frequency range being analyzed was about 0.01–0.20 Hz in Fairfield and Ness (1970), 0.003–0.25 Hz in Luhmann et al. (1986), 0.02–1.0 Hz in Shevyrev and Zastenker (2005), and 0.1–2 Hz in Dimmock et al. (2014). It is unclear whether and how the differences in the ULF frequency ranges have affected the dependence of magnetosheath fluctuations on the solar wind. The current paper therefore divides the fluctuations into three ULF ranges, 0.001–0.01 Hz, 0.01–0.1 Hz, and 0.1–1 Hz, and develops the functional form for each range to understand the sensitivity of frequency.

2. Data Set

2.1. Selecting Subsolar Magnetosheath Intervals

Fluctuations in the magnetosheath are studied using THEMIS A magnetic field measurements taken from 2008 to 2023 by the fluxgate magnetometer (FGM) (Auster et al., 2008). Data of the 4 Hz FGM resolution are used because they provide adequate sampling frequency for ULF fluctuations and sufficient coverage for a statistical analysis. We mainly focus on the subsolar magnetosheath, as fluctuations in this region have a high probability reaching the magnetopause and affecting the dayside solar wind-magnetosphere interaction. Intervals of subsolar magnetosheath are selected based on the spacecraft location, measured magnetic field, and plasma moments automatically. Ion differential energy spectra would serve as a better parameter than plasma moments for event selection as they contain higher-order information about the energy distribution of particles but they are not used in the current study because of the large data size (4–9 times larger). Spacecraft is deemed to be located in the magnetosheath if it meets meet the following criteria simultaneously.

A. Outside the magnetosphere: the spacecraft was located outside the magnetopause estimated by the Shue et al. (1998) model.
B. Outside the magnetosphere: plasma beta at the spacecraft should be larger than 0.5, which is the lower limit of the 5%–95 % range for magnetosheath plasma beta (Cassak & Fuselier, 2016) and is larger than the typical beta inside the magnetosphere.
C. Behind the bow shock: ion speed at the spacecraft should be less than 80% of the prevailing solar wind speed.
D. Subsolar check: the angle between the spacecraft positional vector and the GSM x-axis, that is, the solar zenith angle, is less than 30°.

We use the Shue et al. (1998) model because this model was frequently used in previous magnetosheath fluctuation studies (e.g., Dimmock et al., 2014, 2016; Gutynska et al., 2015; Pi et al., 2024; Shevyrev & Zastenker, 2005). Using the same model help to construct a database that is consistent with prior studies, as well as to cross-compare the results. However, because the modeled magnetopause location is subject to uncertainty, Criterion B is invoked to exclude instances when the spacecraft was actually located inside the magnetosphere. Criterion C selects intervals when the spacecraft is located behind the bow shock where the solar wind has been decelerated. The requirement of 80% accommodates fast structures in the magnetosheath, such as high speed jets which have a dynamic pressure larger than half of that of the solar wind (Plaschke et al., 2013). Although the threshold of 80% may falsely include foreshock intervals (e.g., Xirogiannopoulou et al., 2024) our database is overall insensitive to the specific choice of the threshold. For instance, a requirement of less than 50% of the solar wind speed would reduce the sample size by <10%, which has a limited effect on the median property of the magnetosheath. Criterion D limits the spacecraft to the subsolar region. In addition, we impose the following two criteria on the continuity of measurements:

E. Spacecraft was located in the subsolar magnetosheath continuously for an hour or longer.
F. The instruments were operated in fast survey mode, providing magnetic field measurements at 4 Hz continuously for half an hour or longer.

Criterion E focuses on situations where spacecraft was in the magnetosheath for extended period without entering/exiting the boundary because the motion of the boundary causes apparent fluctuations in the time series of magnetic field measurements that may not relate to fluctuations inside the magnetosheath. Criterion F selects long data record at the cadence of our interest. The choice of half an hour is because we characterize magnetosheath fluctuations based on 30-min windows (see Section 2.2). The OMNI solar wind data are also required to be available for ≥70% of time for each magnetosheath interval.

2.2. Characterizing Magnetic Field Fluctuations

Magnetic fluctuations are first extracted by applying a bandpass filter to the magnetic field data series. The passband frequency ranges are 0.001–0.01 Hz, 0.01–0.1 Hz, and 0.1–1 Hz, which we refer to low, mid, and high frequency in the present paper. The fluctuations are then segmented with a sliding 30 min interval with a step size of 15 min. We chose 30 min because the size of the window should be sufficiently long to accommodate fluctuations on the lower frequency end of ULF fluctuations, which is 1,000 s (about 17 min) in the current paper. It should also be sufficiently short so that the magnetosheath conditions do not change drastically over the duration of the window. The fluctuations, denoted by B_f, are separated into components which are parallel ($B_\parallel$) and perpendicular ($B_\perp$) to the background magnetic field direction $\widehat{\boldsymbol{b}_o}$. This is achieved by first determining the direction of $\widehat{\boldsymbol{b}_o}$ with the following equation:

$$\widehat{\boldsymbol{b}_o} = \frac{\left[\overline{B_X}, \overline{B_Y}, \overline{B_Z}\right]}{\sqrt{\overline{B_X}^2 + \overline{B_Y}^2 + \overline{B_Z}^2}}$$

Where $\overline{B_X}, \overline{B_Y}, \overline{B_Z}$ represent the 30-min averaged magnetic field in the GSM coordinates in the X, Y, Z direction respectively. The parallel component, $B_\parallel$, is then determined as the projection of $\boldsymbol{B_f}$ along $\widehat{\boldsymbol{b}_o}$:

$$B_\parallel = \boldsymbol{B_f} \cdot \widehat{\boldsymbol{b}_o}$$

And the perpendicular component $B_\perp$ is calculated by subtracting $B_\parallel$ from $\boldsymbol{B_f}$:

$$B_\perp = \boldsymbol{B_f} - \widehat{\boldsymbol{b}_o} B_\parallel$$

$B_\parallel$ and $B_\perp$ represent magnetosheath fluctuation at one instance of time, and the mean characteristics of the fluctuations are computed as the root mean square of $B_\parallel$ and $B_\perp$ over the 30-min window as follows.

$$\overline{B_\parallel} = \sqrt{\sum_{i=1}^{N} |B_\parallel|_i^2 / N}$$

$$\overline{B_\perp} = \sqrt{\sum_{i=1}^{N} |B_\perp|_i^2 / N}$$

Where N represents the number of data points in the 30-min window. Each $\overline{B_\parallel}$ and $\overline{B_\perp}$ is recorded as one sample in our statistical analysis and we have obtained 3,936 samples. The location of the spacecraft in the GSM coordinates during these samples are shown in Figures 1a–1c.

2.3. Determining the Prevailing Solar Wind Conditions

The solar wind conditions are determined using the OMNI database (http://omniweb.gsfc. nasa.gov), which propagates solar wind and IMF conditions at various upstream locations, often around the L1 point, to the bow

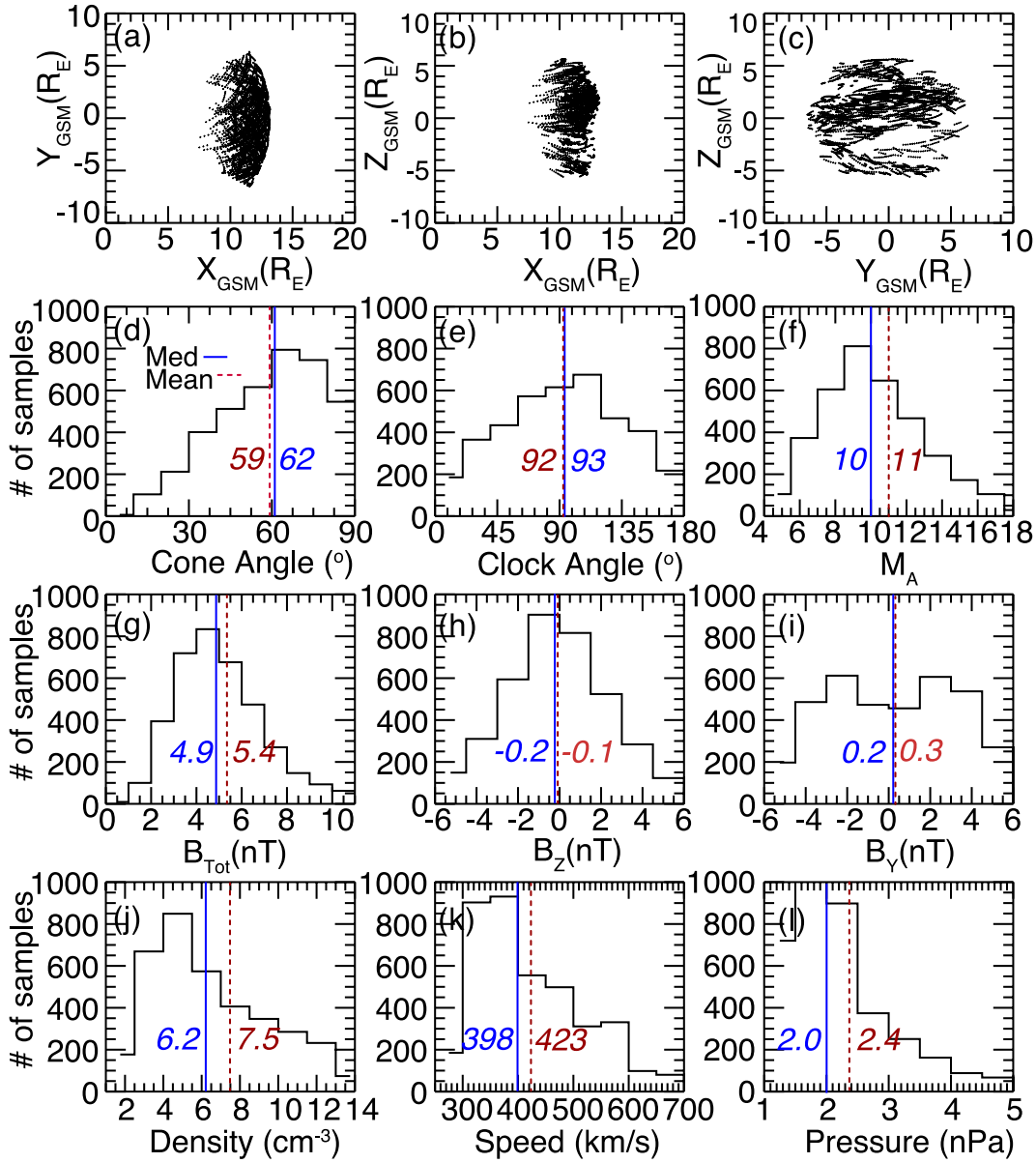

Figure 1. (a–c) Location of THEMIS A spacecraft in the GSM coordinates when magnetosheath samples were taken. (d–l) Histograms showing the distribution of the number of samples as a function of various solar wind parameters. The studied parameters include the IMF cone angle, the IMF clock angle, the Alfvén Mach number, the IMF strength, the IMF B_Z and B_Y components, the solar wind density, speed, and dynamic pressure. The median and mean value of each quantity is drawn as the vertical solid blue and dotted red line, respectively, and the corresponding values are also shown blue and red.

shock nose (King & Papitashvili, 2005). The condition corresponding to each $\overline{B_{\parallel}}$ and $\overline{B_{\perp}}$ is determined as averages of the solar wind parameters in the 30-min window that was used to compute $\overline{B_{\parallel}}$ and $\overline{B_{\perp}}$ (also $\widehat{\boldsymbol{b}_o}$). We have not considered the delay between the arrival of the solar wind at the bow shock nose and its effect at the spacecraft location inside the magnetosheath. This is because such delay is on the order of several minutes (Yu & Ridley, 2011), much shorter than the 30-min size of the window used to characterize the solar wind or the magnetosheath.

Figures 1d–1l present histograms of the solar wind parameters for the statistical data set. The distributions of the parameters are typical of expected solar wind parameters. The cone angle in Figure 1d is defined as the angle between the IMF direction and the Sun-Earth line, and the IMF has its most common configuration as quasi-

perpendicular (60°–90°), and least common configuration as quasi-parallel (0°–30°). The clock angle in Figure 1e is defined as the angle of between the IMF in the plane perpendicular to the Sun-Earth line and the GSM north direction. Normally a clock angle of 0° (180°) indicates a northward (southward) IMF, and 90° (270°) indicates a duskward (dawnward) IMF. This, however, means that as the clock angle increases, it changes discontinuously from 360° down to 0° at purely northward IMF, creating a problem when computing the average value of the clock angle. We therefore follow the practice adopted in compiling the solar wind-magnetosphere coupling functions where the clock angle is defined as

$$\theta_{\text{clock}} = \tan^{-1}(|B_Y|/B_Z)$$

As the clock angle increases, it first increases from 0° to 180° and then decreases from 180° down to 0°. The IMF tends to have a larger B_Y than B_Z component (more data points within [45°, 135°] range than outside).

The most common Alfvén Mach number is roughly 9 (Figure 1f). The most common total magnetic field is roughly 4 nT (Figure 1g). The B_Z component has a common value of 0 nT (Figure 1h). The B_Y components have a bimodal distribution with peaks at about ±2 nT (Figure 1i). The most common solar wind density and dynamic pressure are roughly 5 cm^{-3} and 2 nPa (Figures 1j and 1l), respectively, and the solar wind speed 400 km s^{-1} (Figure 1j).

Note that spatial variation of magnetosheath fluctuations is not considered in this study. Given our focus on the subsolar region (see Criterion D, the solar zenith angle being less than 30°), spatial variation primarily manifests as variation over radial distance across the magnetosheath. The radial variation trend of magnetosheath fluctuations depends on the source of the fluctuations, and studies have found that fluctuations are slightly larger at larger radial distance (Dimmock et al., 2014). However, the radial variation is generally smaller than the variation associated with the driving solar wind conditions and the local properties of the shock (Fairfield & Ness, 1970; Němeček et al., 2002). Furthermore, an accurate determination of the relative position of spacecraft with respect to the magnetosheath boundaries is challenging. The boundaries are often estimated based on empirical models, and these models can be subject to uncertainties of on the order of one R_E (Case & Wild, 2013; Merka et al., 2003; Staples et al., 2020). Such uncertainties are comparable to the thickness of the subsolar magnetosheath (typically ~4 R_E thick). The fluctuations under analysis should hence be viewed as averages across the magnetosheath radial profile.

3. Results

3.1. Dependence of Magnetosheath Fluctuations on Individual Solar Wind Parameters

We first visually examine how magnetosheath fluctuations vary with solar wind parameters. All solar wind parameters presented in Figure 1 are investigated, with an additional parameter that characterizes the level of fluctuations in the solar wind. This is because fluctuations in the solar wind have been recognized as one potential source of magnetosheath fluctuations (Fairfield & Ness, 1970). The parameter is defined as

$$\Delta B/\overline{B} = \sqrt{\Delta B_X^2 + \Delta B_Y^2 + \Delta B_Z^2}\Big/\overline{B} \quad (1)$$

Where $\overline{B}$ represent the averaged magnitude of the IMF over the 30-min average window, and ΔB_X, ΔB_Y, ΔB_Z represent the standard deviation of the X, Y, Z component of the IMF from $\overline{B}$, respectively. Solar wind parameters that are visually correlated with the magnetosheath fluctuations are presented in Figures 2–4. Those without clear correlations are presented in Figures S1–S3 in Supporting Information S1.

Figure 2 presents the dependence of the magnetosheath fluctuations in the high frequency range (0.1–1 Hz) on the solar wind parameters. Columns from left to right represent the parallel component, the perpendicular component, and the common logarithm of the ratio of the perpendicular to parallel component of the fluctuations. A positive (negative) value of the common logarithm means that the fluctuations are dominated by the perpendicular (parallel) component. Data are only shown when sample size for a given solar wind parameter value exceeds 50. The number 50 is selected to maximize the range of the solar wind conditions covered by our database while

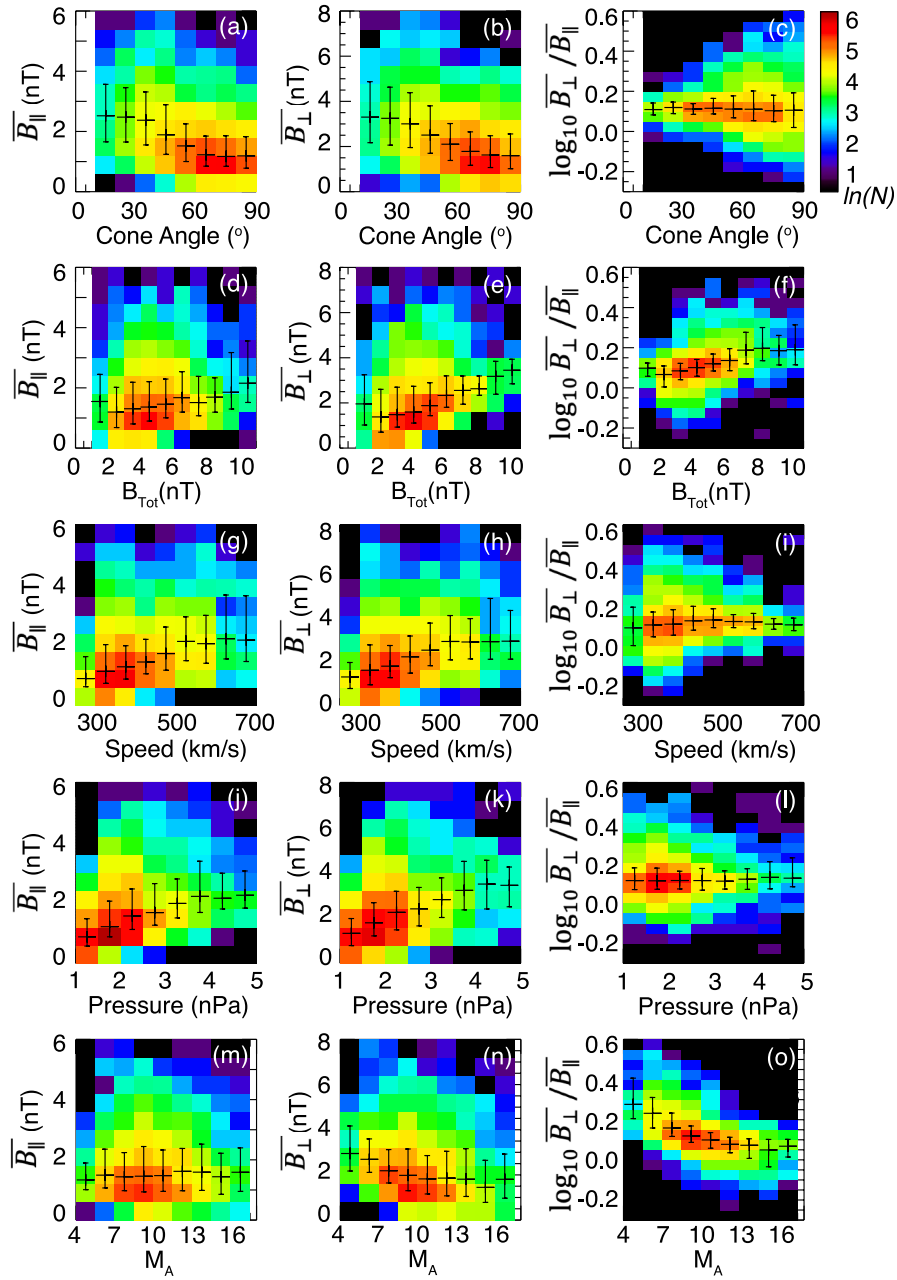

Figure 2. Dependence of the amplitude of high-frequency (0.1–1 Hz) magnetosheath magnetic field fluctuations on various solar wind parameters. The presented solar wind parameters include the IMF cone angle (Panels a–c), the total IMF strength (d–f), the solar wind speed (g–i), the dynamic pressure (j–l), and Mach number (m–o). The left (middle) column is for parallel (perpendicular) fluctuations, and the right column is the common logarithm of the ratio of the perpendicular to parallel component of the fluctuations. The color represents the number of samples. The plus signs and associated error bars represent the median and upper and lower quartile of the amplitude of the fluctuations for a given solar wind parameter.

excluding very rare conditions, rarity meaning less than 10% of the peak sample occurrence for all solar wind parameters (Figure 1).

Consistent with earlier reports, magnetosheath fluctuations in Figures 2a–2c are negatively correlated with the cone angle, with the largest amplitude occurring during the smallest cone angle. The perpendicular component overall exceeds the parallel component. The ratio of the two components does not seem to vary with the cone angle, except for having smaller variance at smaller cone angle.

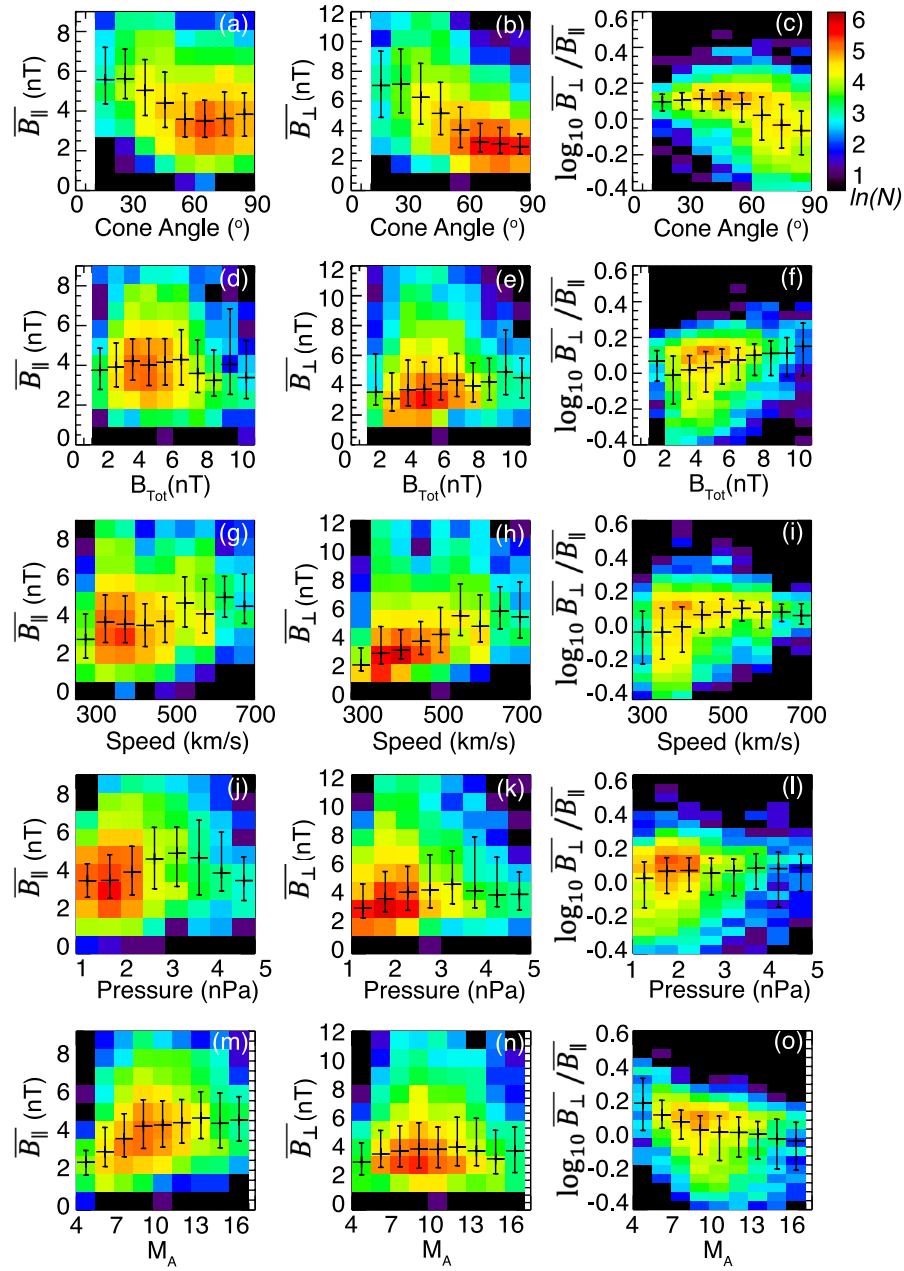

Figure 3. Similar to Figure 2 but for mid-frequency (0.01–0.1 Hz) magnetosheath fluctuations.

Other solar wind parameters also affect magnetosheath fluctuations. Fluctuations tend to increase with the total IMF strength as shown in Figures 2d and 2e, and the increase is more noticeable for the perpendicular than the parallel component. As a result, the ratio of the two components increases with the IMF. Fluctuations also increase with the solar wind speed up to around 500 km/s and stay elevated as shown in Figures 2g and 2h. The larger fluctuations during faster solar wind are consistent with Dimmock et al. (2014). One explanation is that fast solar wind is associated with high-speed jets (Kramer et al., 2025), foreshock transients (Liu et al., 2017), and interplanetary discontinuities (Tsurutani & Ho, 1999), which can drive the magnetosheath magnetic field to vary. High speed jets and foreshock transients also tend to occur during low cone angles (Zhang et al., 2022 and references therein). The dependence on the solar wind dynamic pressure in Figures 2j and 2k is likely related to that on the solar wind speed as the pressure is proportional to the speed squared.

Alfvenic Mach number is negatively correlated with the perpendicular component up to around 10, whereas it shows little relation with the parallel fluctuations (Figures 2m and 2n). The latter could be related to the fact the Mach number is the ratio of the solar wind speed to the Alfven speed. Both parameters are positively correlated with the fluctuations (Figures 2d and 2g), and taking their ratio neutralizes the effect. This also explains the negative correlation of Mach number with the perpendicular fluctuation component because this component increases with IMF (and hence the Alfven speed) more quickly than the parallel component (Figure 2f). Physically, we speculate that part of the perpendicular fluctuations is contributed by EMIC waves, and EMIC waves have been shown to develop preferentially at small Mach number (see Section 4.2). The ratio of the perpendicular to the parallel components decreases with Mach number, meaning that the fraction of compressional fluctuations is larger for higher Mach number.

We now discuss fluctuations in the mid frequency range (0.01–0.1 Hz) and compare to those high frequency (0.1–1 Hz) ones. Although magnetosheath fluctuations still negatively correlate with the IMF cone angle (Figures 3a and 3b), the dependence on other solar wind parameters is noticeably different from high frequency. The dependence on the IMF strength is very subtle and shows large scatter, and the increase with the solar wind dynamic pressure occurs at a much slower speed than that of high frequency. For the parallel component, the dependence on the solar wind speed is not as monotonical (Figures 2g and 2h), suggestive of a weaker correlation. The most interesting difference is the dependence on the Mach number. The parallel fluctuations at high frequency do not exhibit a dependence on the Mach number, while here they increase with the Mach number up to 9 and stay elevated. The perpendicular fluctuations at high frequency decrease with the Mach number, whereas here they show little dependence. We speculate that part of the parallel fluctuations is contributed by mirror mode waves, and mirror mode waves have been shown to develop preferentially at large Mach number (see Section 4.2). Part of the parallel fluctuations could also originate from upstream foreshock waves, which have a typical period of 30s (right within the mid frequency range) (e.g., Turc et al., 2023), and those waves tend to occur at a high Mach number. On the other hand, the ratio of the two components suggests that magnetosheath fluctuations are populated more with compressional fluctuations at larger Mach number, and this trend is consistent with the high frequency.

Another potentially interesting feature is that mid frequency fluctuations are larger at smaller absolute value of the IMF B_Y component and the IMF transverse component (component perpendicular to the Sun-Earth line, see Figure S2 in Supporting Information S1). This trend is more significant for the parallel than perpendicular component. Furthermore, mid frequency fluctuations have a sharp drop in occurrence below an amplitude of 1 nT for a wide range of solar wind conditions, which is different from other frequency bands. The cause warrants further analysis.

Fluctuations in the low frequency range (0.001–0.01 Hz) continue to show a strong correlation with the IMF clock angle (Figures 4a and 4b). The slightly weaker fluctuations at a clock angle of 10–20° is probably not statistically significant because of the relatively small number of events there. Note that there are fewer samples for fluctuations in the lower than higher frequency range because our data are processed with a bandpass filter. Filters in general tend to produce distorted output at the beginning and end of the section of filtered data, known as the edge effects. We measure the length of the edge as half of the maximum wavelength of the filter (which is 500 s in this case) and exclude the edges from analysis. A filter of lower frequency is associated with a longer length of edge, and hence fewer usable samples. Low frequency fluctuations contain 2,854 samples, as opposed to 3,936 samples of high frequency fluctuations.

The parallel component shows little dependence on the IMF total strength (Figure 4d). It is positively related to the solar wind speed and the dynamic pressure (Figures 4g and 4j), although for the latter the dependence stops at around 3.5 nPa. It increases with the Mach number when M_A is less than 7 (Figure 4m). The perpendicular component is still positively related to the IMF strength as well as the solar wind speed (Figures 4b and 4e). It increases with the solar wind dynamic pressure under small pressure conditions (<2.5 nPa, Figure 4h). It appears to decrease with the Mach number, although the trend is non-monotonic (Figure 4n).

The low frequency fluctuations exhibit an additional clear dependence on the level of fluctuations in the solar wind (Figures 4p and 4q). Such dependence may shed light on the origin of magnetosheath fluctuations: low frequency magnetosheath fluctuations may commonly originate from the solar wind, but the mid or high frequency ones do not. It is noteworthy mentioning that the solar wind fluctuations are computed based on 1-min OMNI measurements that do not contain information of fluctuations in the mid or high frequency ranges.

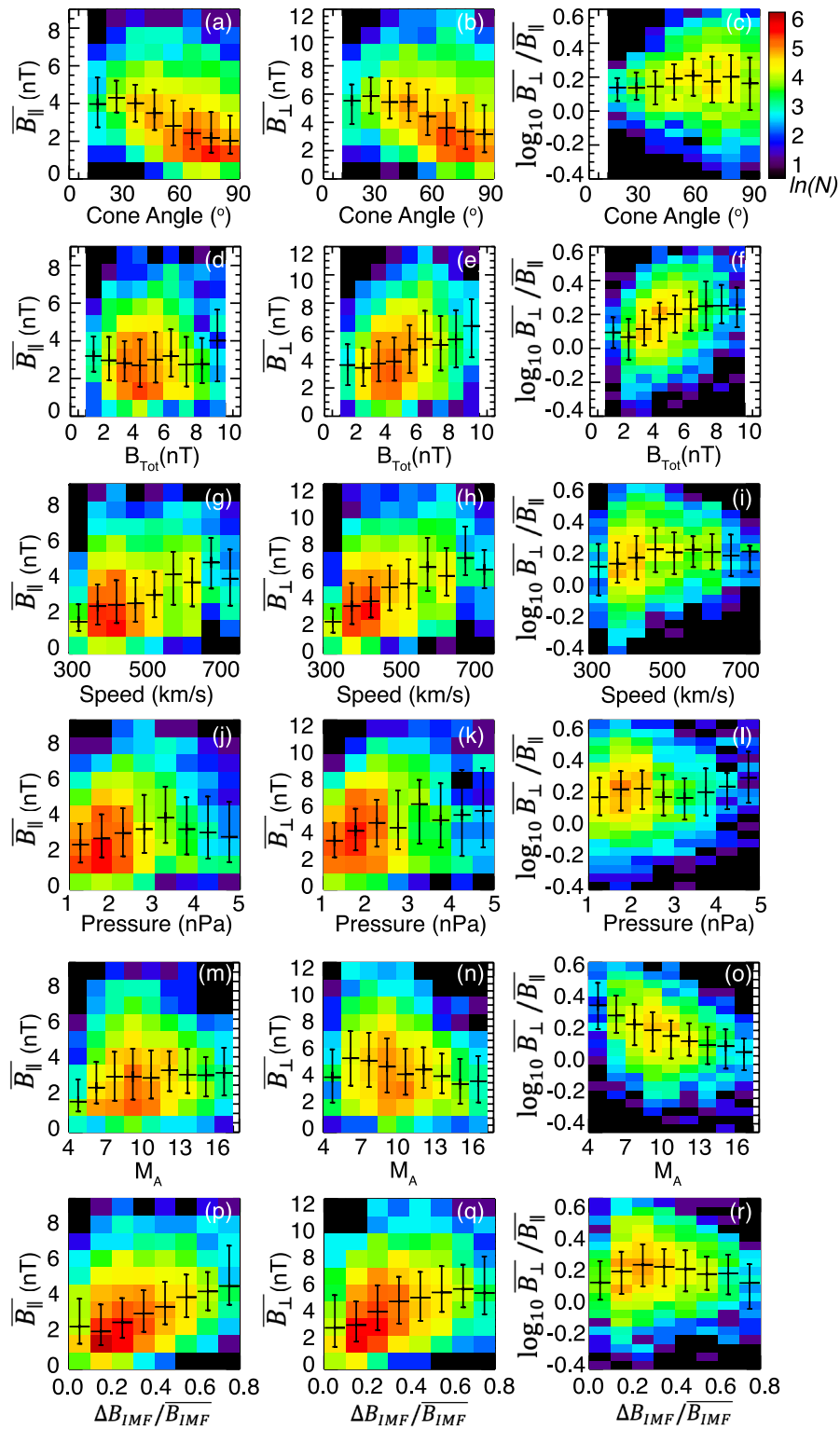

Figure 4. Similar to Figure 2 but for low-frequency (0.001–0.01 Hz) magnetosheath fluctuations. Here the fluctuations are additionally shown as a function of the fluctuation level in the solar wind (Panels p–r).

Table 1
Linear Correlation Coefficients Between Magnetosheath Magnetic Field Fluctuations and Individual Solar Wind Parameters

	0.1–1 Hz		0.01–0.1 Hz		0.001–0.01 Hz	
	$\overline{B_{\parallel}}$	$\overline{B_{\perp}}$	$\overline{B_{\parallel}}$	$\overline{B_{\perp}}$	$\overline{B_{\parallel}}$	$\overline{B_{\perp}}$
$\sin(\overline{\theta_{cone}})$	−0.36	−0.35	−0.31	−0.50	−0.33	−0.29
$\overline{B_{IMF}}$	0.24	0.40	−0.07	0.12	0.01	0.26
$\overline{V}$	0.39	0.40	0.19	0.40	0.28	0.40
$\overline{P_{dyn}}$	0.54	0.49	0.26	0.27	0.22	0.25
$\overline{M_A}$	0.02	−0.20	0.22	−0.01	0.09	−0.17
$\sin(\overline{\theta_{clock}}/2)$	−0.09	−0.10	−0.07	−0.05	−0.03	−0.02
$\overline{B_{IMF,T}}$	−0.01	0.13	−0.22	−0.16	−0.16	0.04
$\overline{n}$	0.10	0.05	0.05	−0.11	−0.06	−0.12
$\Delta B_{IMF}/\overline{B_{IMF}}$	0.14	0.06	0.13	0.19	0.35	0.37
Functional form	0.54	0.62	0.35	0.61	0.54	0.66

Note. The presented parameters include the IMF cone angle, the total IMF strength, the solar wind speed, dynamic pressure, Alfven Mach number, the IMF clock angle, the transverse component of the IMF, the solar wind number density, and the level of fluctuations in the IMF. The last row shows the correlation coefficient with the fitted functional form of magnetosheath fluctuations, as obtained from multiple linear regression. Correlation coefficients that are larger than 0.2 are highlighted in red.

However, using 1-s ACE magnetic field data still does not improve the correlation (see Section 4.2 below), suggesting that the lack of correlation is probably real.

Overall, the visual inspection has yielded the following key features. (a) The IMF cone angles are negatively correlated with fluctuations. (b) The solar wind speed and dynamic pressure are positively correlated with fluctuations. (c) The correlation between the IMF strength and fluctuations varies with the frequency of the fluctuations, and is stronger for the perpendicular than the parallel component of the fluctuations. (d) The level of fluctuations in the solar wind is positively correlated with <0.01 Hz fluctuations in the magnetosheath. (e) A higher Mach number is associated with a larger fraction of compressional versus transverse fluctuations in the magnetosheath.

3.2. Magnetic Fluctuations as a Function of Combined Solar Wind Parameters

3.2.1. Identifying Correlated Parameters

We use the multiple linear regression model to obtain magnetosheath fluctuations as a function of combined solar wind parameters because the regression model has a simple and concise form (so that it is easy to use) and is one of the most commonly used statistical methods to model the relationship between a dependent variable and one or more independent variables. The model assumes the relation between the dependent and independent variables to be linear, which is only approximately true. For instance, the dependence of magnetosheath fluctuations on the cone angle plateaued beyond 60° in Figures 2–4, and a similar pattern is found in Shevyrev and Zastenker (2005). The dependence on the solar wind speed also plateaued beyond 500 km/s. The physics of the nonlinear dependence remains unclear but the nonlinear feature will be not captured by the regression model. Two steps are taken to obtain the function form. First, we compute the linear correlation coefficients between magnetosheath fluctuations and individual solar wind parameters to determine correlation magnitude. Second, for solar wind parameters that are correlated (referred to as correlated parameters for simplicity), we perform a multiple linear regression fit to determine what combination of the parameters predict magnetosheath fluctuations well.

Table 1 lists the linear correlation efficient between magnetosheath fluctuations and solar wind parameters. Note that we choose the sine function to represent the effect of the cone angle because it is dimensionless, but this choice does not alter the correlation. Also the variables have been transformed to logarithmic scales when computing the correlation coefficient and constructing the multiple linear regression (Section 3.2.2).

The correlation of indiviual parameter is overall weak (<0.5) due to the large scatter of data, which is expected given the assumptions we make. For instance, the 30-min averages of the solar wind conditions may not contain all essential information to account for magnetosheath fluctuations. Correlation between solar wind parameters and magnetosheath fluctuations may not be linear. Moreover, magnetosheath fluctuations may be affected by processes beyond the solar wind (such as the magnetopause, the bow shock, and the foreshock). Measurement limitations also exist. For example, the parcel of solar wind captured in OMNI, which often measured at a location around the L1 point, may not be the same parcel that reaches the Earth. The fluctuations measured at a point location in the magnetosheath may not be representative of the overall fluctuations throughout the magnetosheath. However, while indiviual parameter may be weakly correlated, a combination of these can produce a higher correlation (see below).

We regard a correlation coefficient of 0–0.2 as being nearly non-correlated, and values above 0.2 are considered correlated (albeit weakly) and shown in red in Table 1. The IMF cone angle, solar wind speed and dynamic pressure are correlated with magnetosheath fluctuations across all frequencies, with the exception of solar wind speed in the mid-frequency range that has a 0.19 correlation with parallel fluctuations, but we still classify it as correlated due to the small gap to meet the correlation threshold.

The IMF strength is also correlated with high frequency fluctuations, as well as fluctuations of the perpendicular component in the low frequency range. However, it is not correlated with mid frequency fluctuations or fluctuations of the parallel component in the high frequency range. These fluctuations seem to be slightly better correlated with the transverse component of the IMF (the component in the GSM YZ plane) instead, as most clearly seen for the parallel fluctuations in mid frequency range (Figure S2 in Supporting Information S1). However, as shown below, the fluctuations only vary slowly with the transverse IMF component (power index being 0.12), making this parameter comparatively unimportant in the final functional form. The reason why the IMF strength correlates with some fluctuations not others is unclear at present and warrants further investigation.

The Mach number is negatively correlated with the perpendicular component in the high frequency range, and positively correlated with the parallel component in the mid frequency range. It is also negatively "correlated" with the perpendicular component in low frequency range although this relation is below our threshold of being correlated. The level of solar wind fluctuations is positively correlated with low-frequency magnetosheath fluctuations, and almost correlated with the mid-frequency fluctuations in the perpendicular component.

3.2.2. Constructing the Functional Form

Construction of the functional form for magnetosheath fluctuations requires the input parameters, which are the solar wind parameters, to be independent from each other. Because the solar wind dynamic pressure is dependent on the speed, only one of the two can be used for developing the functional form. We do not find the pressure to be a notably better or worse choice than the speed given their comparable correlation coefficients. However, the pressure is more complex (related to two quantifies: the solar wind mass density and speed), and is typically used less frequently than the solar wind speed in coupling functions (see Newell et al. (2007)), and hence is not adopted here. Similarly, the Mach number is not used because it depends on multiple quantities: the solar wind speed, density, and the IMF strength. Note that although the dynamic pressure and the Mach number do not appear explicitly in the functional form, their effects are still included through the combinations of other solar wind parameters.

It is noteworthy to point out that our IMF fluctuation term $\frac{\Delta B_{\mathrm{IMF}}}{\overline{B_{\mathrm{IMF}}}}$ essentially represents normalized fluctuations, and the normalization is motivated by the fact that larger IMFs tend to have larger amplitude fluctuations. After normalizing, the IMF fluctuation term is mostly independent from the IMF strength, despite the appearance of the IMF strength as the denominator in the expression. In fact, correlation analysis reveals a correlation coefficient of −0.17, which is very weak.

We assume that the magnetosheath fluctuations vary with the solar wind with a functional form of

$$\overline{B} = \sin^{a}\left(\overline{\theta_{\mathrm{cone}}}\right) \cdot \overline{B_{\mathrm{IMF}}}^{b} \cdot \overline{V}^{c} \cdot \left(\frac{\Delta B_{\mathrm{IMF}}}{\overline{B_{\mathrm{IMF}}}}\right)^{d} \cdot e \tag{2}$$

Where e represents a constant. B_{IMF} represents the strength of the total IMF in nanotesla (nT), or the transverse component, depending on which correlates with the fluctuations according to Table 1. If neither is correlated, then b is taken to be zero. V represents the solar wind speed in kilometer per second (km/s). $\frac{\Delta B_{\mathrm{IMF}}}{\overline{B_{\mathrm{IMF}}}}$ represents the level of fluctuations in the solar wind as defined in Equation 1 and is dimensionless. Unknown of a, b, c, d, and e can be derived by first taking the logarithms of both sides of the equation, that is,

$$\log_{10}\overline{B} = a \cdot \log_{10}\sin\left(\overline{\theta_{\mathrm{cone}}}\right) + b \cdot \log_{10}\overline{B_{\mathrm{IMF}}} + c \cdot \log_{10}\overline{V} + d \cdot \log_{10}\frac{\Delta B_{\mathrm{IMF}}}{\overline{B_{\mathrm{IMF}}}} + \mathrm{constant} \tag{3}$$

and then conducting a multiple linear regression fit. The fitting results are shown in Table 2. The parallel component of the mid-frequency fluctuations is fitted twice, with and without the IMF transverse component because although this component is correlated with a coefficient of −0.22, the power index obtained from the fitting is small, being 0.12. This means that fluctuations vary rather slowly with the IMF. We therefore experimented a second fit without the IMF. The absence of IMF does not impair, in fact it slightly improves, the goodness of the fit indicated by the F-value, which is defined as the ratio of variance explained by the regression fit to the unexplained variance. It also yields a more negative regression coefficient of the IMF cone angle. The

Table 2
Coefficients From the Multiple Linear Regression Fit

	0.1–1 Hz		0.01–0.1 Hz			0.001–0.01 Hz	
	$\overline{B_{\parallel}}$	$\overline{B_{\perp}}$	$\overline{B_{\parallel}}$		$\overline{B_{\perp}}$	$\overline{B_{\parallel}}$	$\overline{B_{\perp}}$
a	−0.71	−0.76	−0.28	−0.43	−0.74	−0.80	−0.82
b (for B_{IMF})	0.24	0.52	–	–	–	–	0.44
c	0.82	0.74	0.40	0.33	0.77	0.46	0.46
b (for $B_{IMF,T}$)	–	–	−0.12	–	–	–	–
d						0.33	0.40
e	−2.21	−2.09	−0.43	−0.32	−1.50	−0.68	−0.78
f-value	464.0	763.6	191.9	246.7	1003.5	401.2	517.3

Note. Coefficients are computed only for solar wind parameters that are correlated with magnetosheath fluctuations. Coefficients a–d represent the power index of the IMF cone angle, the total IMF strength, the solar wind speed, and the level of fluctuation in the IMF, respectively. Coefficient e represents the constant, and f-value represents the goodness of the fit.

latter is likely because the IMF transverse component is not completely independent from the cone angle, that is, when the cone angle increases, the transverse component also increases. Inclusion of the IMF transverse component in fitting hence undermines the statistical significance of the cone angle in the variances of magnetosheath fluctuations. We therefore only use the fitting results without the IMF transverse component.

Figure 5 compares magnetosheath fluctuations predicted by the multiple linear regression fit and those observed. Most of the data points are distributed around the black diagonal line that represents a perfect match between the prediction and observation. This demonstrates that the functional form has captured the averaged amplitude of magnetosheath fluctuations quite well for a given solar wind condition. Correlating the functional form to magnetosheath fluctuations has yielded a correlation coefficient in the range of 0.5–0.7 Hz as shown in Table 2 (bottom row, except for parallel fluctuations in the mid frequency range, see paragraph below), suggesting correlation strength above moderate. Figure 5 also shows that significant scatter still occurs and has a larger spread above than below the diagonal line. The scatter may arise from the assumed functional form of magnetosheath fluctuations, where fluctuations are a product of multiplication of solar wind parameters. It can also occur due to magnetosheath fluctuations having spatial dependence. The limitations that have contributed to the somewhat low correlation coefficients may also apply here.

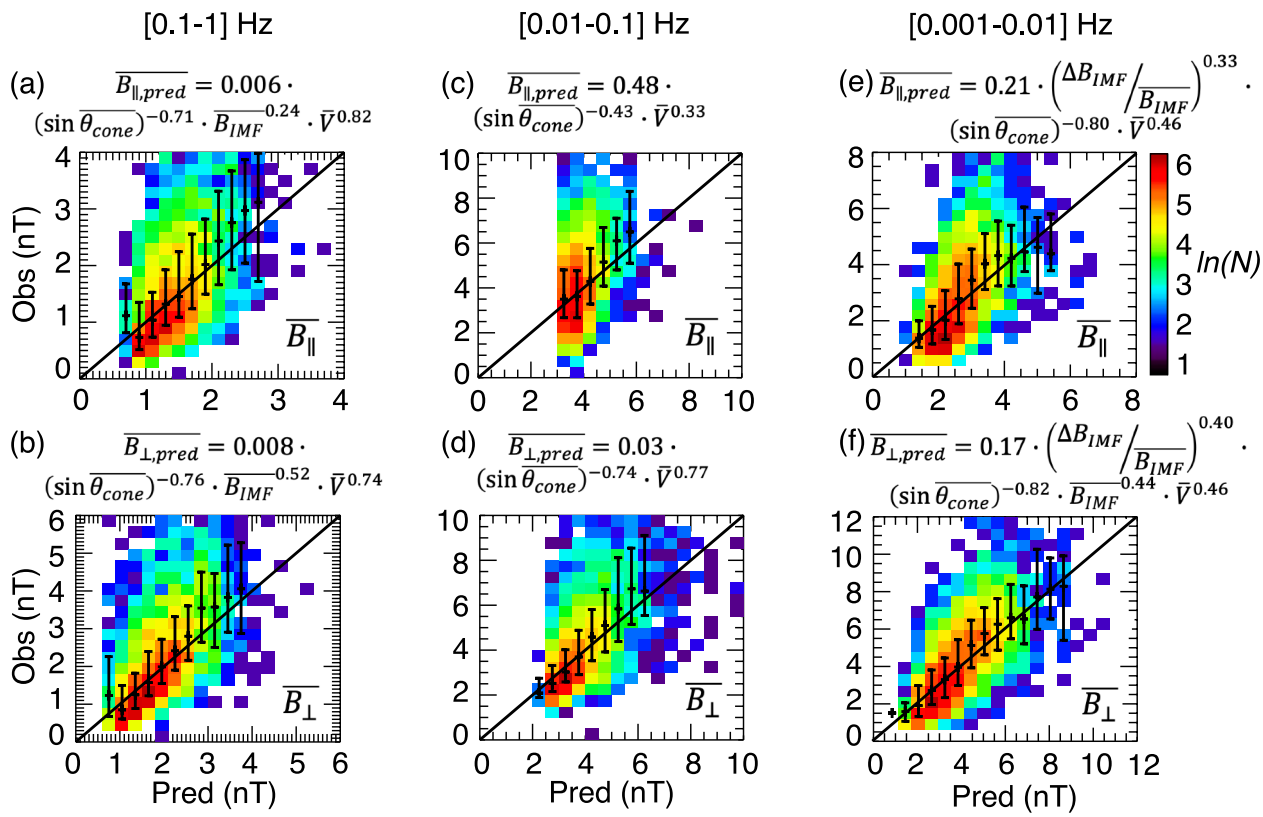

Figure 5. Comparison between observed and predicted amplitude of magnetosheath fluctuations. The prediction is based on the functional form obtained through multiple linear regression, and those functional forms are displayed at the top of each panel. Different columns show fluctuations at different frequencies (Panels a and b for high frequency, c and d for mid frequency, and e and f for low frequency), and the top and bottom rows show the parallel and perpendicular fluctuations, respectively. The color represents the number of samples (blank for no samples), and the plus sign and associated error bars represent the median, and upper and lower quartile of the observed amplitude corresponding to a prediction amplitude. The diagonal line represents a perfect match between observation and prediction. The *P*-value of the correlation is <0.00001.

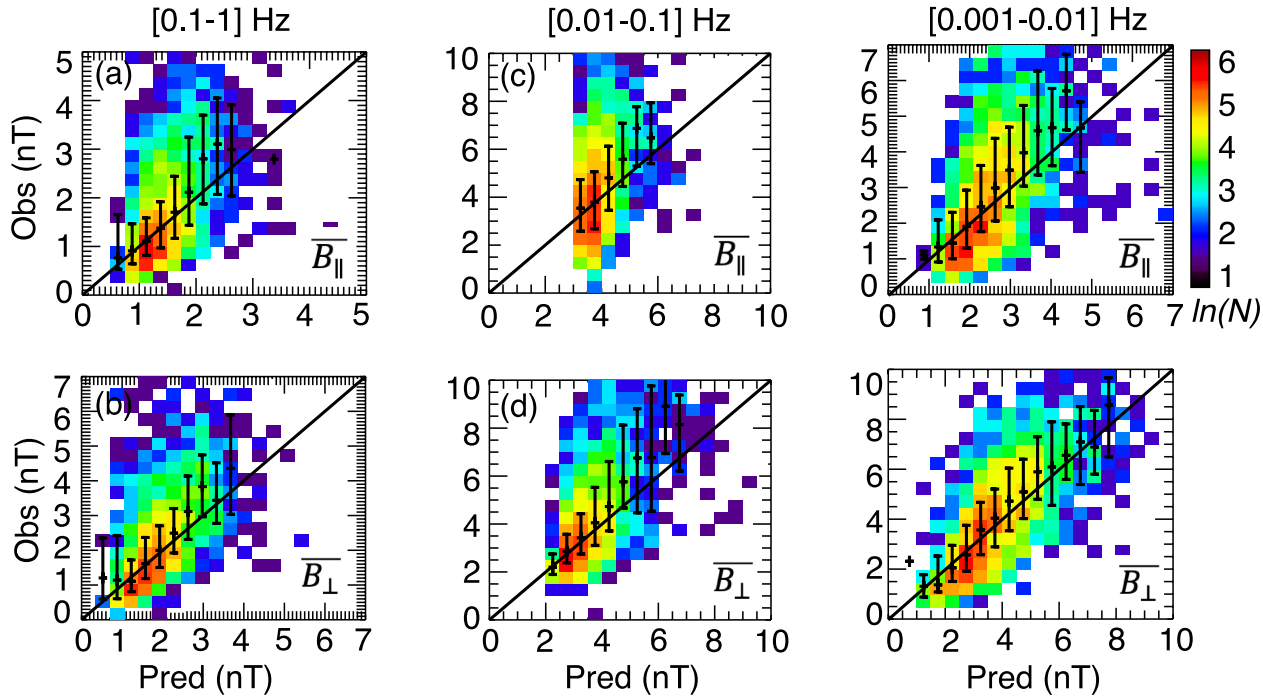

Figure 6. Similar to Figure 5 but for THEMIS E. The prediction is still based on the functional form constructed with THEMIS A data. The *P*-value of the correlation is <0.00001.

Note that the prediction fails to predict <3 nT parallel fluctuations in the mid frequency range. The mid-frequency parallel fluctuations are in general worst represented by the predictions, and an inspection of the regression fitting results show that the power index of the IMF cone angle and solar wind speed are smallest across fluctuations of all frequencies and of both components. This may indicate that the mid-frequency parallel fluctuations are not strongly controlled by the solar wind, or the relation to the solar wind is more complex than the simple functional form proposed here. It leaves an open question with respect to the nature of the mid-frequency parallel fluctuations, but these fluctuations possibly include effects of upstream foreshock waves with a typical period of 30s, and hence may be strongly affected by foreshock conditions.

4. Discussion

4.1. Performance of the Functional Form

To test the function form we developed using THEMIS A probe, we compare it with THEMIS E magnetosheath measurements. Figure 6 shows the comparison between THEMIS E measured magnetosheath fluctuations with the prediction of the functional form developed, where THEMIS E data were processed in the same manner as described in Section 2 for THEMIS A. The level of agreement between prediction and observation is similar to that for THEMIS A, confirming the goodness of our fitting.

The constructed functional form in this study will benefit from future studies that include other missions, such as MMS and Cluster, for a larger sample size and a broader coverage of various solar wind conditions. The larger sample size also allows construction of a functional form that has a more complicated form than the multiple linear regression, and hence address the non-linear dependence of magnetosheath fluctuations on the solar wind. Prediction of magnetosheath fluctuations can also possibly be achieved through supervised machine learning methods, such as neural networks, the result of which can be assessed against the empirical form in this study. In fact, the magnetosheath database can be constructed with unsupervised machine learning (Toy-Edens et al., 2024), which is more robust than the threshold approach we employed in our event selection. When near-Earth upstream measurements are available, they provide better specification of the solar wind conditions than OMNI, especially for small scale structures which may be smoothed out or not accurately mapped from L1. Measurements of the foreshock also elucidate the effect of local bow shock processes that are not represented by

the solar wind on magnetosheath fluctuations. Conjunct measurements of local upstream and downstream conditions may thus improve the prediction at mid/high frequency.

4.2. Source of Magnetosheath Fluctuations

The specific wave mode associated with magnetosheath fluctuations warrants a separate study, and it is very likely that the fluctuations are dominated by a mixture of magnetohydrodynamic waves. This is particularly true for fluctuations behind quasi-parallel shocks because their power spectra often show a broadband shape (Anderson & Fuselier, 1993). Fluctuations behind perpendicular shocks are generally dominated by two wave modes: mirror mode waves and EMIC waves. The two waves usually have a frequency between 0.05 and 1 Hz, which corresponds to mid and high frequency ranges in the current study, and are both generated inside the magnetosheath through instabilities. The difference of the two wave modes is that EMIC (mirror mode) waves are transverse (compressional) waves with magnetic field variations predominantly in the perpendicular (parallel) direction. The fact that Figures 2 and 3 show that magnetosheath fluctuations are dominated by the perpendicular (parallel) component at large cone angle at high (mid) frequency implies that the magnetosheath is likely to be populated with EMIC (mirror mode) waves. Indeed, EMIC waves tend to develop under small Mach number (Soucek et al., 2015), and the perpendicular fluctuating component at high frequency decreases with Mach number. Mirror mode waves tend to develop under high Mach number, and the parallel fluctuating component at mid frequency increases with Mach number.

The fact that low-frequency magnetosheath fluctuations are correlated with the level of fluctuations in the solar wind suggests that the low frequency fluctuations, at least partly, are likely to originate from the solar wind. Studies based on simultaneous measurements in the solar wind and magnetosheath have shown that solar wind or IMF disturbances can indeed pass through the bow shock into the magnetosheath (Zastenker et al., 2002). On the other hand, one may wonder whether the lack of correlation between mid/high frequency magnetosheath fluctuations with the solar wind is due to the low cadence of OMNI measurements that do not contain information of fluctuations in corresponding frequency range. We therefore examine the correlation with time shifted 1-s ACE magnetic field data as follows.

For each magnetosheath fluctuation data sample (which is computed from a 30-min window), we search for corresponding 30-min-long ACE magnetic field. To take into account the time (10s min) the solar wind takes to propagate from the L1 orbit to the bow shock, we use the OMNI spacecraft-specific time shift (if no time shift inference is available, the data sample is excluded from analysis). The level of fluctuations in the solar wind is then characterized in the same manner as for OMNI (Equation 1), except for using 1-s ACE data. As shown in Figure 7, mid/high frequency magnetosheath fluctuations are still not correlated with the fluctuations in the solar wind. We therefore postulate that mid/high frequency fluctuations are significantly contributed by the bow shock and the foreshock processes. The speculation is supported by the dependence of fluctuations on the solar wind speed and the Mach number because fast solar wind and large Mach number favors a variety of foreshock transients as mentioned in Section 3.1.

5. Summary

The study investigates the solar wind control of magnetic field fluctuations of various frequencies in the subsolar magnetosheath based on large statistics of THEMS measurements. The results show that qualitatively, fluctuations are negatively correlated with the IMF cone angle, and positively correlated with the solar wind speed and dynamic pressure. Some fluctuations are correlated with the IMF strength but others show little relation. The level of fluctuations in the IMF is positively correlated with <0.01 Hz fluctuations in the magnetosheath. A higher Mach number is associated with a larger fraction of compressional versus transverse fluctuations in the magnetosheath.

The above relation is quantified via linear correlation coefficient and multiple linear regression fit. The correlation coefficients confirm the finding based on qualitative analysis, and further show that the correlation strength of individual solar wind parameter is less than moderate, all being <0.5. The scatter could arise from effects of time-averaging, and simplified assumptions about the correlation being bivariate as well as linear, and unaccounted effect from the shock/foreshock.

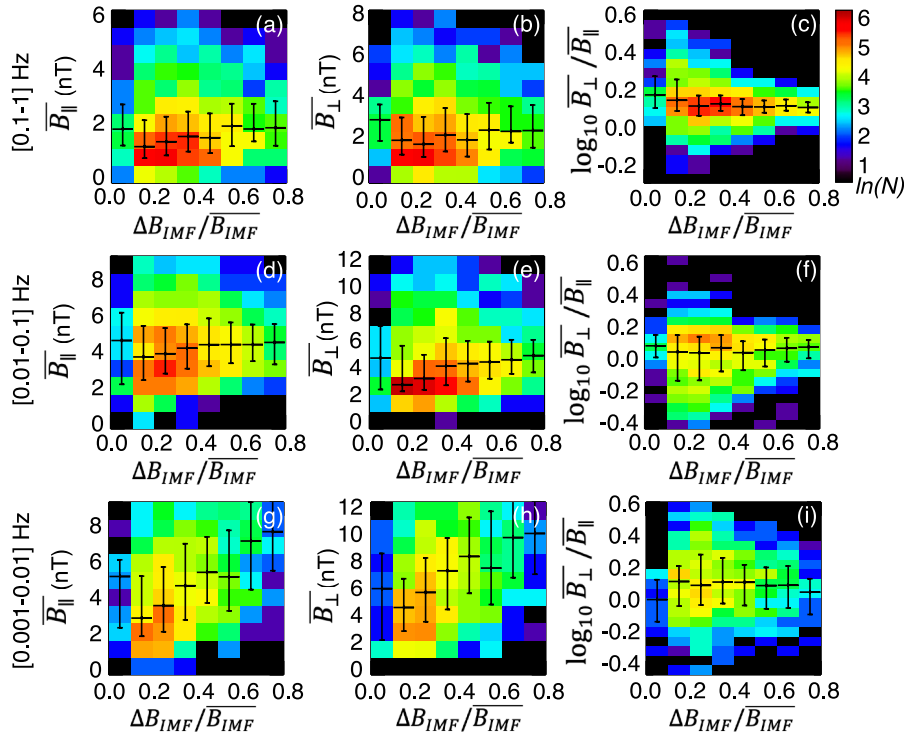

Figure 7. Dependence of magnetosheath fluctuations on the level of fluctuations in the IMF based on ACE 1 s data. The three rows represent magnetosheath fluctuations at different frequency ranges, and the three columns represent parallel fluctuations, perpendicular fluctuations, the common logarithm of the ratio of the perpendicular to parallel component of the fluctuations.

Solar wind parameters that are correlated with magnetosheath fluctuations are used to fit the magnetosheath fluctuations. The fitted combination of solar wind parameters has provided reasonably good prediction of magnetosheath fluctuations with correlation magnitude above moderate, in the range of 0.5–0.7, except for the parallel fluctuations in the 0.01–0.1 Hz frequency range. Scatter still occurs, probably due to the assumed functional form of magnetosheath fluctuations, where fluctuations are a product of multiplication of solar wind parameters, or to magnetosheath fluctuations having spatial dependence.

The solar wind parameters we obtain that affect magnetosheath fluctuations are overall consistent with earlier studies. However, our quantitative approach allows us to use solar wind conditions to estimate the IMF variations in the magnetosheath before the plasma reaches the magnetosphere. Such information is beneficial not only for scientific understanding of the solar wind-magnetosphere understanding, but also for space weather forecasts because it allows small scale fluctuations to be parameterized in MHD models, such as GAMERA/MAGE and BATS-R-US, and assists model validation for hybrid and PIC models.

Data Availability Statement

THEMIS data are available through http://themis.ssl.berkeley.edu/data/themis/. OMNI data are available through https://spdf.gsfc.nasa.gov/pub/data/omni/. ACE data are available through https://izw1.caltech.edu/ACE/ASC/.

Acknowledgments
The work is supported by 80NSSC23K1409. YZ is additionally supported by 80NSSC24K0803. SR acknowledges support from the Johns Hopkins University Applied Physics Laboratory independent R&D fund.

References

Ala-Lahti, M., Pulkkinen, T. I., Brenner, A., Keebler, T., Al Shidi, Q., Hill, S., & Welling, D. (2024). The Impact of solar wind magnetic field fluctuations on the magnetospheric energetics. *Geophysical Research Letters*, *51*(24), e2024GL112922. https://doi.org/10.1029/2024GL112922

Anderson, B. J., & Fuselier, S. A. (1993). Magnetic pulsations from 0.1 to 4.0 Hz and associated plasma properties in the Earth's subsolar magnetosheath and plasma depletion layer. *Journal of Geophysical Research*, *98*(A2), 1461–1479. https://doi.org/10.1029/92JA02197

Auster, H. U., Glassmeier, K. H., Magnes, W., Aydogar, O., Baumjohann, W., Constantinescu, D., et al. (2008). The THEMIS fluxgate magnetometer. *Space Science Reviews*, *141*, 235–264. https://doi.org/10.1007/978-0-387-89820-9_11

Borovsky, J. E., & Funsten, H. O. (2003). Role of solar wind turbulence in the coupling of the solar wind to the Earth's magnetosphere. *Journal of Geophysical Research*, *108*(A6), 1246. https://doi.org/10.1029/2002JA009601

Case, N. A., & Wild, J. A. (2013). The location of the Earth's magnetopause: A comparison of modeled position and in situ Cluster data. *Journal of Geophysical Research: Space Physics*, *118*(10), 6127–6135. https://doi.org/10.1002/jgra.50572

Cassak, P. A., & Fuselier, S. A. (2016). Reconnection at Earth's dayside magnetopause. In *Magnetic reconnection: Concepts and applications* (pp. 213–276).

D'Amicis, R., Bruno, R., & Bavassano, B. (2007). Is geomagnetic activity driven by solar wind turbulence? *Geophysical Journal Letters*, *34*(5), L05108. https://doi.org/10.1029/2006GL028896

Dimmock, A. P., & Nykyri, K. (2013). The statistical mapping of magnetosheath plasma properties based on THEMIS measurements in the magnetosheath interplanetary medium reference frame. *Journal of Geophysical Research: Space Physics*, *118*(8), 4963–4976. https://doi.org/10.1002/jgra.50465

Dimmock, A. P., Nykyri, K., Osmane, A., & Pulkkinen, T. I. (2016). Statistical mapping of ULF Pc3 velocity fluctuations in the Earth's dayside magnetosheath as a function of solar wind conditions. *Advances in Space Research*, *58*(2), 196–207. https://doi.org/10.1016/j.asr.2015.09.039

Dimmock, A. P., Nykyri, K., & Pulkkinen, T. I. (2014). A statistical study of magnetic field fluctuations in the dayside magnetosheath and their dependence on upstream solar wind conditions. *Journal of Geophysical Research: Space Physics*, *119*(8), 6231–6248. https://doi.org/10.1002/2014ja020009

Fairfield, D. H. (1976). Magnetic fields of the magnetosheath. *Reviews of Geophysics*, *14*(1), 117–134. https://doi.org/10.1029/rg014i001p00117

Fairfield, D. H., & Ness, N. F. (1970). Magnetic field fluctuations in the Earth's magnetosheath. *Journal of Geophysical Research*, *75*(31), 6050–6060. https://doi.org/10.1029/ja075i031p06050

Génot, V., Budnik, E., Jacquey, C., Dandouras, I., & Lucek, E. (2009). Mirror modes observed with Cluster in the Earth's magnetosheath: Statistical study and IMF/solar wind dependence. *Advances in Geosciences*, *14*, 263–283. https://doi.org/10.1142/9789812836205_0019

Gutynska, O., Sibeck, D. G., & Omidi, N. (2015). Magnetosheath plasma structures and their relation to foreshock processes. *Journal of Geophysical Research: Space Physics*, *120*(9), 7687–7697. https://doi.org/10.1002/2014JA020880

Hoilijoki, S., Palmroth, M., Walsh, B. M., Pfau-Kempf, Y., von Alfthan, S., Ganse, U., et al. (2016). Mirror modes in the Earth's magnetosheath: Results from a global hybrid-Vlasov simulation. *Journal of Geophysical Research: Space Physics*, *121*(5), 4191–4204. https://doi.org/10.1002/2015JA022026

Karimabadi, H., Roytershteyn, V., Vu, H. X., Omelchenko, Y. A., Scudder, J., Daughton, W., et al. (2014). The link between shocks, turbulence, and magnetic reconnection in collisionless plasmas. *Physics of Plasmas*, *21*(6), 062308. https://doi.org/10.1063/1.4882875

King, J. H., & Papitashvili, N. E. (2005). Solar wind spatial scales in and comparisons of hourly Wind and ACE plasma and magnetic field data. *Journal of Geophysical Research*, *110*(A2). https://doi.org/10.1029/2004ja010649

Krämer, E., Koller, F., Suni, J., LaMoury, A. T., Pöppelwerth, A., Glebe, G., et al. (2025). Jets downstream of collisionless shocks: Recent discoveries and challenges. *Space Science Reviews*, *221*(1), 1–59.

Liu, T. Z., Angelopoulos, V., Hietala, H., & Wilson, L. B., III. (2017). Statistical study of particle acceleration in the core of foreshock transients. *Journal of Geophysical Research: Space Physics*, *122*(7), 7197–7208. https://doi.org/10.1002/2017JA024043

Lu, Q., Wang, H., Wang, X., Lu, S., Wang, R., Gao, X., et al. (2020). TurbulenceDriven magnetic reconnection in the magnetosheath downstream of a quasi-parallel shock: A three-dimensional global hybrid simulation. *Geophysical Research Letters*, *47*(1), e2019GL085661. https://doi.org/10.1029/2019gl085661

Luhmann, J. G., Russell, C. T., & Elphic, R. C. (1986). Spatial distributions of magnetic field fluctuations in the dayside magnetosheath. *Journal of Geophysical Research*, *91*(A2), 1711–1715. https://doi.org/10.1029/JA091iA02p01711

Lyon, J. G. (1994). MHD simulations of the magnetosheath. *Advances in Space Research*, *14*(7), 21–28. https://doi.org/10.1016/0273-1177(94)90043-4

Merka, J., Szabo, A., Narock, T. W., King, J. H., Paularena, K. I., & Richardson, J. D. (2003). A comparison of IMP 8 observed bow shock positions with model predictions. *Journal of Geophysical Research*, *108*(A2), 1077. https://doi.org/10.1029/2002JA009384

Němeček, Z., Šafránková, J., Zastenker, G. N., Pišoft, P., & Jelínek, K. (2002). Low-frequency variations of the ion flux in the magnetosheath. *Planetary and Space Science*, *50*(5), 567–575. https://doi.org/10.1016/S0032-0633(02)00036-3

Newell, P. T., Sotirelis, T., Liou, K., Meng, C.-I., & Rich, F. J. (2007). A nearly universal solar wind-magnetosphere coupling function inferred from 10 magnetospheric state variables. *Journal of Geophysical Research*, *112*(A1), A01206. https://doi.org/10.1029/2006JA012015

Omidi, N., Sibeck, D., Gutynska, O., & Trattner, K. J. (2014). Magnetosheath filamentary structures formed by ion acceleration at the quasi-parallel bow shock. *Journal of Geophysical Research: Space Physics*, *119*(4), 2593–2604. https://doi.org/10.1002/2013JA019587

Osmane, A., Dimmock, A. P., Naderpour, R., Pulkkinen, T. I., & Nykyri, K. (2015). The impact of solar wind ULF B_Z fluctuations on geomagnetic activity for viscous timescales during strongly northward and southward IMF. *Journal of Geophysical Research: Space Physics*, *120*(11), 9307–9322. https://doi.org/10.1002/2015JA021505

Palmroth, M., Ganse, U., Pfau-Kempf, Y., Battarbee, M., Turc, L., Brito, T., et al. (2018). Vlasov methods in space physics and astrophysics. *Living Reviews in Computational Astrophysics*, *4*, 1. https://doi.org/10.1007/s41115-018-0003-2

Paularena, K. I., Richardson, J. D., Kolpak, M. A., Jackson, C. R., & Siscoe, G. L. (2001). A dawn-dusk density asymmetry in Earth's magnetosheath. *Journal of Geophysical Research*, *106*(A11), 25377–25394. https://doi.org/10.1029/2000JA000177

Pi, G., Němeček, Z., Šafránková, J., & Grygorov, K. (2024). Spatial profiles of magnetosheath parameters under different IMF orientations: THEMIS observations. *Frontiers in Astronomy and Space Sciences*, *11*, 1401078. https://doi.org/10.3389/fspas.2024.1401078

Plaschke, F., Hietala, H., & Angelopoulos, V. (2013). Anti-sunward high-speed jets in the subsolar magnetosheath. *Annales Geophysicae*, *31*(10), 1877–1889. https://doi.org/10.5194/angeo-31-1877-2013

Pulinets, M. S., Ryazantsev, M. O., Antonova, E. E., & Kirpichev, I. P. (2012). Dependence of magnetic field parameters at the subsolar point of the magnetosphere on the interplanetary magnetic field according to the data of the THEMIS experiment. *Geomagnetism and Aeronomy*, *52*(6), 730–739. https://doi.org/10.1134/S0016793212060084

Rakhmanova, L., Riazantseva, M., & Zastenker, G. (2016). Correlation level between solar wind and magnetosheath plasma and magnetic field parameters. *Advances in Space Research*, *58*(2), 157–165. https://doi.org/10.1016/j.asr.2015.09.036

Rakhmanova, L., Riazantseva, M., Zastenker, G., & Šafránková, J. (2015). Modification of small- and middle-scale solar wind structures by the bow shock and magnetosheath: Correlation analysis. *Planetary and Space Science*, *115*, 12–18. https://doi.org/10.1016/j.pss.2015.03.003

Russell, C. T., & Elphic, R. C. (1979). ISEE observations of flux transfer events at the dayside magnetopause. *Geophysical Research Letters*, *6*(1), 33–36. https://doi.org/10.1029/GL006i001p00033

Šafránková, J., Hayosh, M., Gutynska, O., Němeček, Z., & Přech, L. (2009). Reliability of prediction of the magnetosheath B component from interplanetary magnetic field observations. *Journal of Geophysical Research*, *114*(A12). https://doi.org/10.1029/2009JA014552

Schwartz, S. J., Burgess, D., & Moses, J. J. (1996). Low-frequency waves in the Earth's magnetosheath: Present status. *Annales Geophysicae*, *14*(11), 1134–1150. https://doi.org/10.1007/s00585-996-1134-z

Shevyrev, N. N., & Zastenker, G. N. (2005). Some features of the plasma flow in the magnetosheath behind quasi-parallel and quasi-perpendicular bow shocks. *Planetary and Space Science*, *53*(1–3), 95–102. https://doi.org/10.1016/j.pss.2004.09.033

Shevyrev, N. N., Zastenker, G. N., & Du, J. (2007). Statistics of low-frequency variations in solar wind, foreshock and magnetosheath: INTERBALL-1 and CLUSTER data. *Planetary and Space Science*, *55*(15), 2330–2335. https://doi.org/10.1016/j.pss.2007.05.014

Shevyrev, N. N., Zastenker, G. N., Nozdrachev, M. N., Němeček, Z., Šafránková, J., & Richardson, J. D. (2003). High and low frequency large amplitude variations of plasma and magnetic field in the magnetosheath: Radial profile and some features. *Advances in Space Research*, *31*(5), 1389–1394. https://doi.org/10.1016/S0273-1177(03)00008-5

Shue, J.-H., Song, P., Russell, C. T., Steinberg, J. T., Chao, J. K., Zastenker, G., et al. (1998). Magnetopause location under extreme solar wind conditions. *Journal of Geophysical Research*, *103*(A8), 17691–17700. https://doi.org/10.1029/98JA01103

Siscoe, G. L., Crooker, N. U., Erickson, G. M., Sonnerup, B. U. Ö., Maynard, N. C., Schoendorf, J. A., et al. (2002). MHD properties of magnetosheath flow. *Planetary and Space Science*, *50*(5–6), 461–471. https://doi.org/10.1016/s0032-0633(02)00026-0

Soucek, J., Escoubet, C. P., & Grison, B. (2015). Magnetosheath plasma stability and ULF wave occurrence as a function of location in the magnetosheath and upstream bow shock parameters. *Journal of Geophysical Research: Space Physics*, *120*(4), 2838–2850. https://doi.org/10.1002/2015JA021087

Spreiter, J. R., Summers, A. L., & Alksne, A. Y. (1966). Hydromagnetic flow around the magnetosphere. *Planetary and Space Science*, *14*(3), 223–253. https://doi.org/10.1016/0032-0633(66)90124-3

Staples, F. A., Rae, I. J., Forsyth, C., Smith, A. R. A., Murphy, K. R., Raymer, K. M., et al. (2020). Do statistical models capture the dynamics of the magnetopause during sudden magnetospheric compressions? *Journal of Geophysical Research: Space Physics*, *125*(4), e2019JA027289. https://doi.org/10.1029/2019JA027289

Toy-Edens, V., Mo, W., Raptis, S., & Turner, D. L. (2024). Classifying 8 years of MMS dayside plasma regions via unsupervised machine learning. *Journal of Geophysical Research: Space Physics*, *129*(6), e2024JA032431. https://doi.org/10.1029/2024JA032431

Tsurutani, B. T., & Ho, C. M. (1999). A review of discontinuities and Alfvén waves in interplanetary space: Ulysses results. *Reviews of Geophysics*, *37*(4), 517–541. https://doi.org/10.1029/1999RG900010

Turc, L., Roberts, O. W., Verscharen, D., Dimmock, A. P., Kajdič, P., Palmroth, M., et al. (2023). Transmission of foreshock waves through Earth's bow shock. *Nature Physics*, *19*(1), 78–86. https://doi.org/10.1038/s41567-022-01837-z

Walsh, B. M., Bhakyapaibul, T., & Zou, Y. (2019). Quantifying the uncertainty of using solar wind measurements for geospace inputs. *Journal of Geophysical Research: Space Physics*, *124*(5), 3291–3302. https://doi.org/10.1029/2019JA026507

Walsh, B. M., Sibeck, D. G., Wang, Y., & Fairfield, D. H. (2012). Dawn-dusk asymmetries in the Earth's magnetosheath. *Journal of Geophysical Research*, *117*, A12. https://doi.org/10.1029/2012JA018240

Wilson, L. B., Koval, A., Szabo, A., Breneman, A., Cattell, C. A., Goetz, K., et al. (2013). Electromagnetic waves and electron anisotropies downstream of supercritical interplanetary shocks. *Journal of Geophysical Research: Space Physics*, *118*(1), 5–16. https://doi.org/10.1029/2012JA018167

Wu, C. C. (1992). MHD flow past an obstacle—Large-scale flow in the magnetosheath. *Geophysical Research Letters*, *19*(2), 87–90. https://doi.org/10.1029/91gl03007

Xirogiannopoulou, N., Goncharov, O., Šafránková, J., & Němeček, Z. (2024). Characteristics of foreshock subsolar compressive structures. *Journal of Geophysical Research: Space Physics*, *129*(2), e2023JA032033. https://doi.org/10.1029/2023JA032033

Yu, Y.-Q., & Ridley, A. J. (2011). Understanding the response of the ionosphere-magnetosphere system to sudden solar wind density increases. *Journal of Geophysical Research*, *116*(A4), A04210. https://doi.org/10.1029/2010JA015871

Zastenker, G. N., Nozdrachev, M. N., NeÄmecÄek, Z., Richardson, J. D., Lepping, R. P., & Mukai, T. (2002). Multispacecraft measurements of plasma and magnetic ÿeld variations in the magnetosheath: Comparison with Spreiter models and motion of the structures. *Planetary and Space Science*.

Zhang, H., Fu, S., Pu, Z., Lu, J., Zhong, J., Zhu, C., et al. (2019). Statistics on the magnetosheath properties related to magnetopause magnetic reconnection. *The Astrophysical Journal*, *880*(2), 122. https://doi.org/10.3847/1538-4357/ab290e

Zhang, H., Zong, Q., Connor, H., Delamere, P., Facskó, G., Han, D., et al. (2022). Dayside transient phenomena and their impact on the magnetosphere and ionosphere. *Space Science Reviews*, *218*(5), 40. https://doi.org/10.1007/s11214-021-00865-0